High-pressure behavior of TiO_2 as determined by experiment and theory

Yahya Al-Khatatbeh,[1] Kanani K. M. Lee,[1,2] and Boris Kiefer[1]

[1]*Department of Physics, New Mexico State University, Las Cruces, New Mexico 88003-8001, USA*
[2]*Department of Geology and Geophysics, Yale University, New Haven, Connecticut 06511, USA*

Using high-resolution synchrotron x-ray powder diffraction we have investigated the structural phase transitions and equations of state of titanium dioxide (TiO_2) under high pressure before and after heating at high temperature. The phase sequence we observe experimentally is as follows: rutile (RT)→columbite (CB) →baddeleyite (MI)→orthorhombic I (OI)→orthorhombic II (OII). The equations of state as determined from our experiments are consistent with previous measurements and computations. The only exception is the OII phase for which we find a significantly lower room-pressure bulk modulus (K_0) of 312 (± 34) GPa and room-pressure volume (V_0) of 25.28 (± 0.35) $Å^3$ as compared to previous experiments. We find that the volume decreases across the OI→OII phase transition at room temperature by ~8.3%, in very good agreement with our static *first-principles* calculations which predict volume changes of 8.2% and 7.6% for local-density approximation and generalized gradient approximation, respectively. This volume collapse is significantly higher than previously determined but consistent with the volume decrease observed in other dioxides across this transition.

PACS number(s): 81.40.Vw, 31.15.A−, 64.70.K−, 61.50.Ks

I. INTRODUCTION

The nature of bonding in titanium dioxide TiO_2 is of interest as it is a superhard material with many industrial applications.[1,2] It is expected that the yield strength of materials increases with increasing pressure either within a single phase or across volume reducing phase transitions.[3] Thus, the possibility of quenching high-pressure phases and maintaining them at ambient pressure can generate novel superhard materials with increased mechanical strength as well as other properties.[4,5] This strategy to synthesize novel superhard materials by quenching high-pressure phases to ambient pressures has been successfully applied to other materials such as c-Si_3N_4.[4,5] Previous measurements on TiO_2 show that the highest-pressure phase OII is quenchable to ambient pressure at least at cryogenic temperatures.[1] Previous experiments on high-pressure TiO_2 polymorphs show that this compound can adopt several different structures: rutile (RT, tetragonal, space group: $P4_2/mnm$), anatase (AN, tetragonal, space group: $I4_1/amd$), brookite (BR, orthorhombic, space group: $Pbca$), columbite (CB, orthorhombic, space group: $Pbcn$), baddeleyite (MI, monoclinic, space group: $P2_1/c$), orthorhombic I (OI, orthorhombic, space group: $Pbca$), fluorite (FL, cubic, space group: $Fm3m$), and cotunnite (OII, orthorhombic, space group: $Pnma$).[1,6–10] In most experimental studies, the starting material is rutile[7] or anatase[1,6,9–12] or brookite.[8] The low-pressure phase transition sequence in all studies at room temperature is RT or AN or BR→CB→MI.[6,7,11] On the other hand, the high-pressure phases (OI, FL, and OII) were only observed after heating at high pressures.[1,9,10] In this study, we have investigated the high-pressure phase diagram and determined the equations of state (EOSs) of TiO_2 phases. We examine the OI→OII phase transition and the associated volume change using both experiments and *first-principles* computations and compare our results to the volume change across the OI and OII transitions in similar dioxides.

II. EXPERIMENTAL METHODS

A polycrystalline sample of 99.9% TiO_2 rutile powder (grain size ranged from ~0.5–2 μm), purchased from Sigma-Aldrich, was used as a starting material in our diamond-anvil cell (DAC) experiments. For low-pressure (up to 17 GPa) and unheated experiments, a mixture of methanol-ethanol-water (16:3:1 by volume) was used as a pressure-transmitting medium.[13] For laser-heated experiments, our sample was mixed with sodium chloride (NaCl) as a pressure medium and pressure calibrant[14,15] (rutile:NaCl about 8:2 by mass). In addition, two to three ruby spheres of 5–10 μm in diameter were loaded into the DAC together with the sample used as an additional pressure calibrant.[16] The uncertainty in pressure was determined by averaging the measured pressures from NaCl and ruby. Except for one experimental run (Table I), no laser absorber was added to the sample chamber as the sample was sufficiently absorbent to the infrared (~1 μm) laser for heating at pressures above 25 GPa as previously observed.[1,10] A rhenium gasket precompressed to a thickness of ~25 μm and drilled with a hole of ~150 μm in diameter was placed between matched 300 μm culet diamonds. We have studied the stability range of TiO_2 phases under different experimental conditions of pressure, temperature, pressure media, or laser absorber and have run five different experiments of TiO_2 samples (Table I). Angle-dispersive x-ray diffraction (XRD) patterns were collected at high pressure, before and after laser heating when applicable (i.e., methanol-ethanol-water pressure medium samples were not heated), as well as on decompression confirm the identity of the phases, and show that the observed compressions for RT, CB, MI, and OI are compatible

TABLE I. The experimental conditions for five runs on TiO_2 samples. There is only one unheated experiment and the rest were heated at different pressures to ~1800 (±200) K. For runs 2, 4, and 5, no laser absorber was used. The stability range for the observed phases in each experiment is also given. For the heated experiments, all diffraction patterns were taken after cooling to room temperature. If not applicable, NA is recorded.

Run	Heating history	Heat absorber	Pressure medium	Phase stability range	Pressure-quenched phases
1	Not heated	NA	Methanol-ethanol-water[a]	RT: 0–15 GPa and few reflections up to 17 GPa (compression); MI: ~12–15 to 17 GPa (compression); CB: 8–0 GPa (decompression)	RT and CB
2	Heated to ~1800 K at ~25 GPa	Without absorber	NaCl[b]	RT: few reflections from 20 to 29 GPa (compression, preheat); MI: 20–35 GPa (compression, preheat), 35–25 GPa (decompression, preheat), 25–40 GPa (compression, postheat), and 20–8 GPa (decompression, postheat); OI: 25–42 GPa (compression, postheat) and from 42–20 GPa (decompression, postheat)	CB
3	Heated to ~1800 K at ~43 GPa	Au[c]	NaCl[b]	MI: stable at 43 GPa (compression, preheat) and one reflection from 43 to 37 GPa (decompression, postheat); OI: 2 observed reflections at 43 GPa (preheat) and from 43 to 37 GPa (decompression, postheat)	CB
4	Heated to ~1800 K at ~56 GPa	Without absorber	NaCl[b]	MI: 56–58 GPa with smaller volume (compression, preheat) and from 17 to 12 GPa (decompression, postheat); OI: 56–58 GPa (compression, preheat); OII: 56 GPa (compression, postheat) and 56–12 GPa (decompression, postheat)	CB
5	Heated to ~1800 K at ~49 GPa	Without absorber	NaCl[b]	MI: stable at 60 GPa with smaller volume (compression, preheat) and from 22 to 9 GPa (decompression, postheat); OI: two to three reflections at 60 GPa (compression, preheat); OII: 49 GPa (compression, postheat) and 49–22 GPa (decompression, postheat)	CB

[a]Reference 13.
[b]References 14 and 15.
[c]Reference 36.

with known equations of state (Table II).[1,6,7,10,11] In the laser-heated experiments, samples were compressed and transformed under quasihydrostatic conditions (NaCl) in a laser-heated DAC and characterized at room temperature by synchrotron XRD using a MAR345 image plate at the HP-CAT beamlines (λ=0.3694, 0.3875, 0.4369, or 0.4565 Å) at the Advanced Photon Source at Argonne National Laboratory. Samples were laser heated for ~5–7 min up to ~1800 (±200) K at 25(±1.8) and 56(±0.1) GPa as determined by spectroradiometry[17] (Figs. 1 and 2). In separate experiments, the samples were also heated on compression at ~1800 (±200) K at 43(±1.5) and 49(±3.6) GPa. The laser heat-

ing functioned as both a way to anneal the sample (to minimize deviatoric stress) as well as to add thermal energy to the system in order to overcome possible kinetic barriers due to coordination changes in the synthesis of other phases. All XRD measurements presented, whether laser heated or not, were taken at room temperature. Fit2d[18] was used to integrate collected two-dimensional raw data into one dimension. Volumes were determined using 5–9 reflections for RT, 4–9 reflections for CB, 6–9 reflections for MI, 9–16 reflections for OI, and 4–11 reflections for OII. A Birch-Murnaghan[19,20] fit was used to determine the EOS of each TiO_2 phase (Table II).

TABLE II. The equations of state of the TiO$_2$ phases. All EOSs were obtained from fitting a second-order Birch-Murnaghan equation of state [Eq. (1) with K_0'=4] to our experimental results in order to determine the zero-pressure volume/f.u. TiO$_2$ (V_0) and the isothermal bulk modulus (K_0) for RT, CB, and MI. The EOSs for OI and OII were obtained from a (G versus g) Birch-Murnaghan fit (Refs. 19 and 20). For comparison, we list other experimental results. 1σ uncertainties are given in parentheses.

Phase	V_0 (Å^3)	K_0 (GPa)	K_0'	Ref.
Rutile	31.20(0.01)	235 (10)	4 (fixed)	This work, expt.
	31.25(0.06)	230 (20)	6.6 (0.7)	Expt.[a]
	31.20(0.01)	216 (2)	7 (fixed)	Expt.[b]
Columbite	30.53(0.09)	253 (12)	4 (fixed)	This work, expt.
	30.59(0.08)	258 (8)	4.1 (0.3)	Expt.[c]
Baddeleyite	28.06(0.16)	298 (21)	4 (fixed)	This work, expt.
	28.06(0.16)	290 (10)	4 (fixed)	Expt.[c]
	28.06(0.05)	304 (6)	3.9 (0.2)	Expt.[d]
	27.62(0.01)	303 (5)	3.9 (0.2)	Expt.[e]
OI	27.54(0.13)	314 (16)	4 (fixed)	This work, expt.
	27.27(0.02)	318 (3)	4 (fixed)	Expt.[f]
OII	25.28(0.35)	312 (34)	4 (fixed)	This work, expt.
	26.27(0.05)	431 (10)	1.35 (0.1)	Expt.[d]

[a]Reference 7.
[b]Reference 37.
[c]Reference 6.
[d]Reference 1.
[e]Reference 11.
[f]Reference 10.

The third-order Birch-Murnaghan EOS is given by[19]

$$P = \frac{3}{2}K_0\left[\left(\frac{V}{V_0}\right)^{-7/3} - \left(\frac{V}{V_0}\right)^{-5/3}\right]$$
$$\times\left\{1 + \frac{3}{4}(K_0'-4)\left[\left(\frac{V}{V_0}\right)^{-2/3}\right] - 1\right\}, \quad (1)$$

where P is the applied pressure, V is the volume, V_0 is the zero-pressure volume, K_0 is the zero-pressure bulk modulus, and K_0' is the first pressure derivative of the bulk modulus at zero pressure. As the pressure is the first volume derivative of the energy (E), $P=-\partial E/\partial V$, $P(V)$ form of Eq. (1) can be rewritten in the following $E(V)$ form:

$$E = \frac{9K_0V_0}{2}\left\{\frac{1}{2}\left[\left(\frac{V}{V_0}\right)^{-2/3} - 1\right]^2\right\}\left[1 + (K_0'-4)\right.$$
$$\times\left.\left\{\frac{1}{2}\left[\left(\frac{V}{V_0}\right)^{-2/3} - 1\right]\right\}\right\} + E_0, \quad (2)$$

where E_0 is the zero-pressure energy. A second-order Birch-Murnaghan EOS is given by fixing K_0' to 4 in Eqs. (1) and (2). Our experimental and theoretical data for TiO$_2$ phases were fitted using the second-order Birch-Murnaghan EOS.

III. THEORETICAL METHODS

We augmented our experiments with static *first-principles* calculations to investigate the TiO$_2$ phase diagram. In particular, we were interested in the volume change across the OI→OII transition. The calculations were performed within the framework of density-functional theory (DFT).[21] Interactions between the atoms were treated within the projector augmented wave (PAW) formalism,[22,23] core radii of 2.782 bohr (valence configuration: $3s3p4s3d$) and 2.265 bohr (valance configuration: $2s2p$) for titanium and oxygen, respectively. Electronic exchange and correlation effects were treated at the local-density approximation (LDA) (Ref. 24) and the generalized gradient approximation (GGA) (Ref. 25) levels. All calculations were performed with the VASP software package[22,26] with an energy cutoff of 600 eV and standard k-point meshes.[27] Total energies within one phase and among different phases were converged to better than $\sim$1 meV/atom. In detail, the following k-point meshes were used for the various TiO$_2$ phases in this study: $6\times6\times8$ for RT, $6\times6\times3$ for AN, $6\times4\times6$ for CB, $4\times4\times4$ for MI, $2\times4\times4$ for OI, and $4\times8\times4$ for OII. For all phases, the internal degrees of freedom and lattice parameters were relaxed simultaneously to find the electronic ground state. For each of the TiO$_2$ phases, the ground state was determined for 8–12 volumes that encompassed the experimentally observed pressure range. For the OII phase the highest pressure investigated in our study was 116 GPa (109 GPa) for GGA (LDA), which is well above our experimentally measured OI→OII transition pressure. The EOS was determined by fitting our calculated total energy-versus-volume curve to a Birch-Murnaghan EOS (Ref. 19) [Eq. (2) with K_0'=4], whereas the pressure-versus-volume fit [Eq. (1) with K_0'=4] was used for MI and OII phases in the GGA computations where a minimum in the total energy of these two phases was not well defined most likely due to instabilities of these phases at low pressure. However, as our main interest was the determination of the OI→OII transition pressure, we interpolated the high-pressure enthalpy values computed from the second-order Birch-Murnaghan EOS (Table III).

IV. RESULTS AND DISCUSSION

A. Diamond-anvil cell experiments

In run 1 (Table I), we observed RT stable up to $\sim$15 GPa (e.g., Ref. 7); however, a few low-intensity rutile diffraction peaks were also observed up to $\sim$29 GPa (run 2, Table I) for unheated samples indicating a small kinetic barrier between RT and MI. At $\sim$12 GPa, reflections from the MI phase appear in addition to the RT peaks. The intensity of the MI peaks increases for pressures greater than 15 GPa indicating that MI becomes the stable phase at pressures of 12–15 GPa and remains so up to $\sim$35 GPa (run 2, Table I) at room temperature [Fig. 1(a)]. Upon decompression from $\sim$17 GPa, MI transforms to the CB phase at $\sim$8 GPa. Our quenched XRD pattern at ambient conditions shows only diffraction peaks from RT and CB, demonstrating that MI does not quench at room temperature.

In run 2 (Table I), upon compression at ambient temperature to $\sim$35 GPa, MI was observed to be the stable phase,
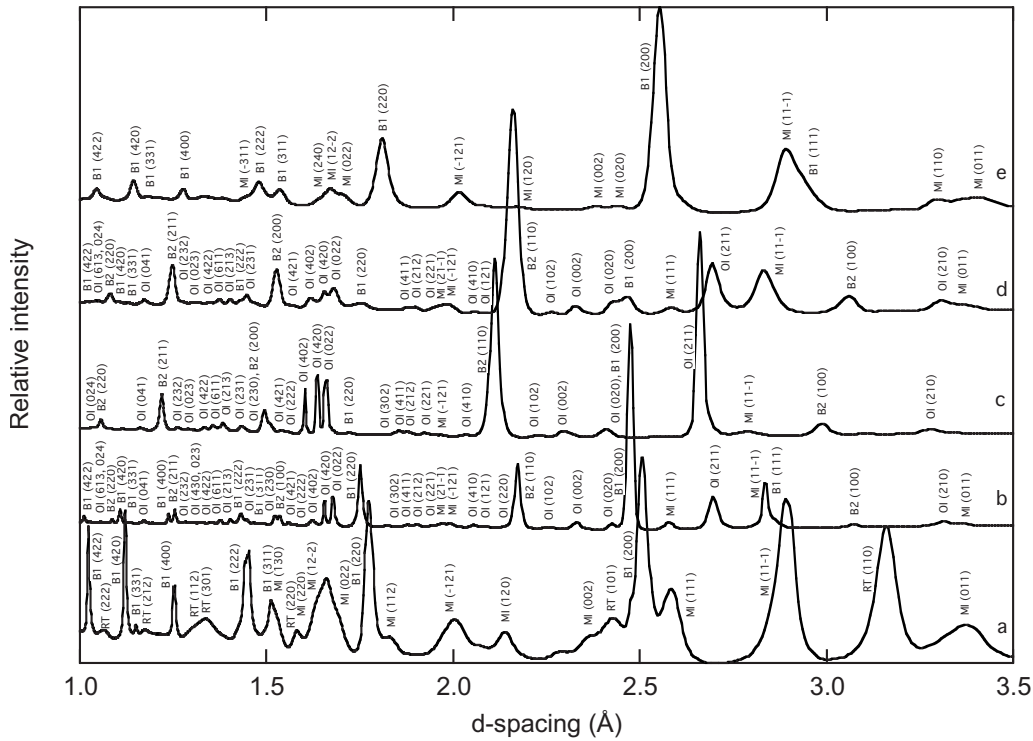
FIG. 1. X-ray diffraction patterns at various pressures during run 2 show rutile (RT), baddeleyite (MI), orthorhombic I (OI), low-pressure phase NaCl (B1), and high-pressure NaCl (B2) corresponding Miller indices. (a) On compression at 20 GPa (preheat), (b) on compression after heating at ~1800 K at 25 GPa, (c) on compression at 42 GPa (postheat), (d) on decompression at 29 GPa (postheat), and (e) on decompression at 16 GPa (postheat).

and few reflections from RT were also observed from 20 to ~29 GPa. Upon decompression from ~35 to ~25 GPa, MI was the only observed phase. After heating the sample to ~1800 (±200) K at ~25 (±1.8) GPa, we observe MI and OI diffraction peaks. A few reflections from MI are still observed despite the high pressure,[6,7,11] although this is likely due to an incomplete transformation [Fig. 1(b)]. Upon further compression, OI diffraction peaks become more intense and MI peaks decrease in intensity and eventually disappear at pressures greater than 40 GPa [Fig. 1(c)]. Upon decompression from 42 GPa, OI remains stable at pressures above ~20 GPa; at lower pressures the MI reflections gain intensity under pressures down to ~8 GPa where CB is the only phase that is observed in the quenched x-ray pattern.

In run 3 (Table I), after heating the sample at ~43 (±1.5) GPa to ~1800 (±200) K, MI partially transforms to OI where only one reflection from MI is still observed upon decompression to ~37 GPa, and upon direct decompression to zero pressure, CB is again the only quenched phase. In the synthesis of OI, even after heating the sample at different pressures (25 GPa in run 2 and 43 GPa in run 3), we notice a partial transformation in both cases, the transformation to OI at 43 GPa is more complete as only one reflection from MI is observed in the x-ray pattern. On the other hand, at 25 GPa, we notice a sluggish transformation, likely due to kinetics, as more reflections from MI are still observed. This is likely due to increased stability of OI at high pressure.

In run 4 (Table I), upon compression to ~58 GPa at ambient temperature, OI was observed [Fig. 2(a)]. In contrast to previous experiments, this indicates that the high-pressure OI

phase can be synthesized at room temperature without heating[10] and that phase boundary between MI and OI has a negative Clapeyron slope. We also observe two unidentified peaks which may be attributed to an unknown phase [indicated by asterisks in Fig. 2(a)] although as there are many peaks in the diffraction pattern, overlapping peaks may mask other potential reflections of this unidentified phase. An alternative explanation is that these two peaks, along with other peaks hidden under the reflections of the more dominant OI phase, belong to the MI phase. However, the *d* spacing would indicate a smaller volume (by ~2%) for MI at this pressure than extrapolated from the EOS (Table II). However, it is difficult to rule out the MI phase due to potentially unusual behavior at pressures far outside of the MI stability range. After heating the sample to ~1800 (±200) K at ~56 (±0.1) GPa, the OI phase and the unidentified two peaks completely disappeared, and the peaks in the diffraction pattern can all be identified as either OII peaks or those of the NaCl pressure medium. During decompression, x-ray peaks of the MI phase reappear at a pressure of ~17 GPa, in addition to peaks from OII. As the sample is further decompressed, reflections from MI become more intense while OII reflections decrease in intensity. At pressures below ~12 GPa, MI and OII both transform to CB. As in the synthesis of OI (described above), we find only CB reflections in the room-temperature pressure-quenched x-ray pattern.

In run 5 (Table I), the sample was compressed at ambient temperature to ~60 GPa; MI was observed to be stable, but with a smaller volume than expected, again indicative of the unusual behavior of MI outside of its stability range. In ad-

TABLE III. The calculated equations of state parameters of the TiO_2 phases as obtained from our LDA and GGA calculations. Our calculations were fit to a second-order Birch-Murnaghan equation of state to find V_0 and K_0 [Eqs. (1) and (2) with $K_0'=4$] (Ref. 19). For comparison, we list other theoretical results. 1σ uncertainties are given in parentheses. For values not available, NA is recorded.

Phase	V_0 (Å^3)	K_0 (GPa)	K_0'	Ref.
Rutile	30.47 (0.01)	250 (2)	4 (fixed)	This work (LDA)
	32.18 (0.02)	216 (2)	4 (fixed)	This work (GGA)
	33.10	243	NA	(LCAO)[a]
	30.45	241 (10)	NA	(LCAO-LDA)[b]
	31.89 (0.01)	215 (1)	5.35 (016)	(GGA)[c]
Anatase	33.64 (0.08)	146 (3)	4 (fixed)	This work (LDA)
	35.65 (0.09)	131 (3)	4 (fixed)	This work (GGA)
	36.20	194	NA	(LCAO)[a]
	33.70	195 (10)	NA	(LCAO-LDA)[b]
Columbite	29.97 (0.07)	212 (9)	4 (fixed)	This work (LDA)
	31.75 (0.05)	188 (4)	4 (fixed)	This work (GGA)
	30.96	247	NA	(LCAO)[a]
	30.70	264 (10)	NA	(LCAO-HF)[b]
	31.30 (0.15)	250 (23)	2.64 (0.70)	(GGA)[c]
Baddeleyite	28.01 (0.01)	190 (2)	4 (fixed)	This work (LDA)
	29.96 (0.04)	157 (1)	4 (fixed)	This work (GGA)
	29.33	249	NA	(LCAO)[a]
	NA	300 (10)	NA	(LCAO-HF)[b]
OI	27.02 (0.04)	236 (3)	4 (fixed)	This work (LDA)
	28.71 (0.04)	209 (2)	4 (fixed)	This work (GGA)
	28.31 (0.06)	272 (9)	3.38 (0.19)	(B3LYP)[c]
OII	24.44 (0.04)	300 (6)	4 (fixed)	This work (LDA)
	25.97 (0.10)	261 (7)	4 (fixed)	This work (GGA)
	26.14	306	4.57	(LDA)[d]
	23.81	341	3.85	(LDA)[e]
	25.38	281	4.8	(GGA)[e]
	NA	380 (10)	NA	(LCAO-HF)[b]

[a]Reference 38.
[b]Reference 34.
[c]Reference 39.
[d]Reference 40.
[e]Reference 41.

dition, two to three reflections from OI were also observed in the preheated sample. After heating to 1800 (±200) K at ∼49 (±3.6) GPa, MI and OI transform both to OII, but one reflection from MI is still observed demonstrating that the transformation to OII is incomplete. Upon decompression, OII remains stable up to ∼22 GPa, where at this pressure, MI is also observed to be stable. At pressures less than 22 GPa, MI remains stable up to ∼9 GPa, where at decompression to room pressure, CB is again the only phase observed.

The different synthesis conditions of OII discussed above show that MI and OI transform to OII completely the first time (run 4) and incompletely during the second attempt (run 5). During run 4, the sample was heated at a higher pressure (56 GPa versus 49 GPa), and the sample was kept at ∼1800 (±200) K for a longer time, suggesting that OII becomes more stable at higher pressures after overcoming a kinetic barrier. This inference is consistent with previous experiments performed on TiO_2.[1]

B. Experimental equation of state determination

We determined the second-order Birch-Murnaghan EOS [Eq. (1) with $K_0'=4$] for pressure-quenchable RT and CB, and for MI phase, we have used the V_0 from previous work[6] to determine the second-order Birch-Murnaghan EOS (Ref. 19) (Table II, Fig. 3). The remaining phases, in addition to MI, are not pressure-quenchable phases, thus we have used the G versus g formulation to find the second-order Birch-Murnaghan EOS.[19,20] For RT, CB, MI, and OI phases, the determined EOSs are in good agreement with previous
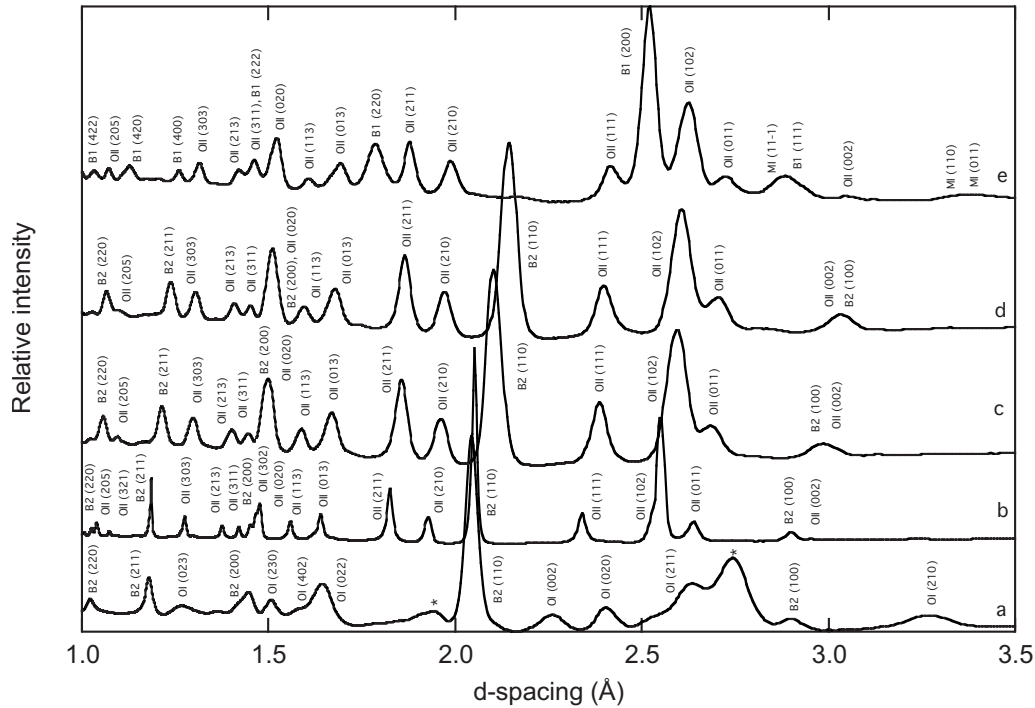
FIG. 2. X-ray diffraction patterns at various pressures during run 4 show baddeleyite (MI), orthorhombic I (OI), orthorhombic II (OII), low-pressure phase NaCl (B1), and high-pressure NaCl (B2) corresponding Miller indices. Unidentified peaks are marked with an asterisk *. (a) On compression at 58 GPa (preheat), (b) on compression after heating at ~1800 K at 56 GPa, (c) on decompression at 37 GPa (postheat), (d) on decompression at 29 GPa (postheat), and (e) on decompression at 18 GPa (postheat).

work.[1,6,7,10,11] This is not the case for the OII phase, where V_0 and K_0 are significantly lower than what has been previously found.[1] This difference may result from different synthesis conditions.[1] To compare, if we fix K_0' to 4 instead of 1.35 from Ref. 1, then K_0 would be ~358 GPa instead of 431 GPa which is still higher than our value (312 GPa) by ~15%, and outside our generous uncertainties, although not unreasonable. The large uncertainties in our EOS determination of OII likely result from using results from two different synthesis conditions (runs 4 and 5), evident in a kink in the volume evolution around 40 GPa as shown in Figs. 3 and 4(f). However, irregardless of our choice of K_0' in our comparison to Ref. 1 and corresponding V_0 and K_0, it is clear from the measured volumes that there is a significant offset between our results and those of Ref. 1 [Fig. 4(f)].

Previous work on the OII phase[1] did not observe the OI transformation to OII as we have, but if we assume that OI (Ref. 10) transforms to OII at the same pressure we have observed (~56 GPa), the volume change at the transition pressure would be ~2.6%. On the other hand, our volume change at the transition pressure between OI and OII is significantly larger, ~8.3%. This large collapse in the volume is not unusual for similar dioxides[28–32] (SnO$_2$, PbO$_2$, ZrO$_2$, and HfO$_2$) (Table IV); i.e., the volume change at the transition pressure between OI and OII is large and compare well with our results than with previous observations on OII.[1,10] Additionally, at ambient conditions, our OII is denser than MI by ~9.9% which compares well again with previous observations on similar dioxides[29] (Table IV) than what has been previously observed on TiO$_2$.[1]

At room temperature, reflections from RT persist up to ~29 GPa (run 2), although its stability range is less than 17

GPa where MI starts to be stable.[7] To determine the EOS for RT, we fit a second-order Birch-Murnaghan EOS for all points up to 29 GPa and for points up to 17 GPa, and K_0 is found to be 234 ($\pm$9) GPa and 235 ($\pm$10) GPa, respectively. As the EOSs are similar, we report the latter EOS as this is when the MI is in its stability range (Table II).

The OI phase becomes stable after heating even though reflections from OI are observed at room temperature and very high pressures, ~56 and 58 GPa [Fig. 2(a)], as discussed previously. Including these two unheated data points
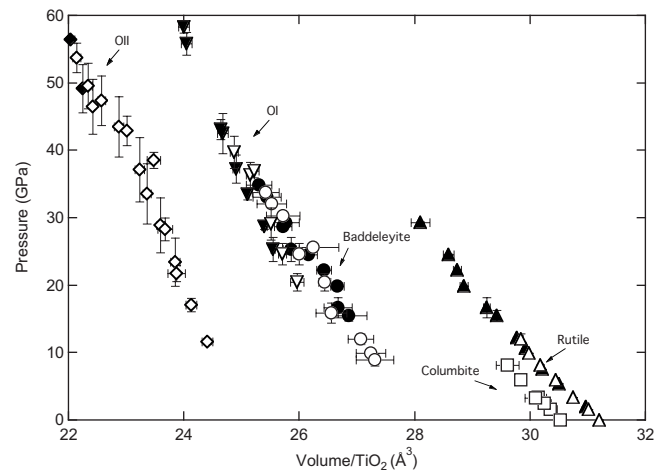

FIG. 3. Pressure versus volume of one TiO$_2$ unit for RT (triangles), CB (squares), MI (circles), OI (inverted triangles), and OII (diamonds). The solid symbols indicate points under compression and open symbols indicate points upon decompression.
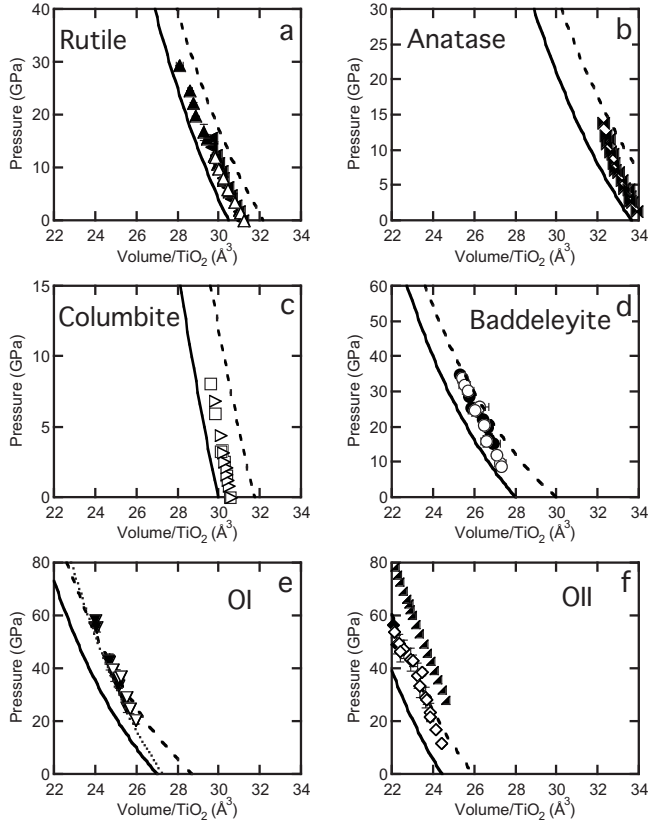
FIG. 4. Pressure versus volume for TiO$_2$ phases. Filled symbols correspond to measurements taken on compression, while open symbols correspond to measurements taken on decompression. Curves show predictions based on LDA (solid) and GGA (dashed) calculations. (a) Rutile: our experimental measurements (triangles); Ref. 7 (left-handed triangles). (b) Anatase: experimental measurements from previous work (Ref. 6) (horizontal bowties) lie in between our GGA and LDA computations. (c) Columbite: our experimental results (squares) are in good agreement with previous observations (Ref. 6) (right-handed triangles). The experimental data points lie in between our GGA and LDA computations. (d) Baddeleyite: our experimental data points (circles) lie in between our GGA and LDA computations at low pressures and get closer to GGA points at higher pressures. (e) OI: our experimental data points (inverted triangles) lie closer to GGA computations especially at pressures higher than 40 GPa; Ref. 10 (dotted curve). (f) OII: our experimental results (diamonds) disagree with previous measurements (Ref. 1) (right-angled triangles). However, our experimental data points are in good agreement with our GGA calculations especially in the pressure range where OII is stable, above ~25 GPa. Our experimental results are in good agreement with previous measurements on RT (Ref. 7), CB (Ref. 6), MI (Refs. 6 and 11), and OI (Ref. 10), but for the OII phase, there is a shift in our volumes relative to volumes previously measured (Ref. 1).

into the second-order Birch-Murnaghan EOS fit gives V_0 of 27.49 ($\pm$0.15) Å^3 and K_0 of 322 ($\pm$20) GPa. On the other hand, if we take these points out and include only the points after heating, we find a V_0 of 27.54 ($\pm$0.13) Å^3 and a K_0 of 314 ($\pm$16) GPa. As OI is observed to be more stable after heating, we report the latter values (Table II). Even so, the EOSs are similar with overlapping uncertainties.

TABLE IV. Experimentally observed change in volume between OI and OII phases of TiO₂ at the transition pressure and the difference in volume between OII and MI at ambient conditions compared to similar dioxides. For values not available, NA is recorded.

Oxide	Change in volume at the transition pressure from OI to OII (%)	Difference in volume between OII and MI at ambient conditions (%)
TiO₂, this work	8.3	9.9
TiO₂ [a]	2.6	6.4
SnO₂ [b]	11	NA
PbO₂ [c]	7.5	NA
ZrO₂ [d,e]	5.8, 9	12.4, 14[f]
HfO₂ [d,g]	7.4, 8	12.4, 15

[a]References 1 and 10.
[b]Reference 30.
[c]Reference 28.
[d]Reference 29.
[e]Reference 31.
[f]V_0 of MI phase of ZrO₂ was taken from Ref. 29.
[g]Reference 32.

As mentioned previously, OII was synthesized at high pressures and temperatures, and two separate experiments were performed for this purpose by heating the sample at 56 (run 4) and 49 (run 5) GPa. At 56 GPa the transformation to OII was complete. In contrast, if heated at 49 GPa, the transformation was incomplete. To determine our EOS for OII, the second-order Birch-Murnaghan EOS fit was taken for all points from both experiments and leads to values V_0 of 25.36 ($\pm$0.42) Å^3 and K_0 of 305 ($\pm$37) GPa. Since the transformation to OII was incomplete when heated at 49 GPa and this phase is stable at high pressures, we only consider the highest-pressure data points from this experiment in our Birch-Murnaghan fit to find V_0 of 25.28 ($\pm$0.35) Å^3 and K_0 of 312 ($\pm$34) GPa. We report the latter values of the EOS due to stability of OII, although both EOSs are similar with overlapping uncertainties (Table II).

C. First-principles computations

Figure 4 shows the experimental data for TiO$_2$ phases compared to our LDA and GGA computations. For low-pressure phases, RT, AN,[6] and CB, the experimental data lie between LDA and GGA computations [Figs. 4(a)–4(c)]. MI is an intermediate phase between the low-pressure phases (RT and CB) and the high-pressure phases (OI and OII). At pressures less than 20 GPa, our experimental data for MI are between our LDA and GGA results. However, the pressure dependence of the experimental volumes is very similar to our GGA results at higher pressures [Fig. 4(d)]. Furthermore, the coordination of titanium in both the MI and OI structures is sevenfold, thus it is not unexpected that the EOSs of both phases are similar. Our measurements of OI [Fig. 4(e)] and OII [Fig. 4(f)] are very similar to the results of our GGA calculations. The systematic change in the compressional behavior may be related to differences in bonding between

TABLE V. Change in volume between OI and OII phases of TiO_2 at transition pressure compared to similar oxides (Ref. 35).

Oxide	Change in volume at transition pressure from OI to OII (%)	
	LDA	GGA
TiO_2, this work	8.2	7.6
ZrO_2 [a]	NA	10.5
HfO_2 [a]	10.4	9.9

[a]Reference 35.

low-pressure and high-pressure TiO_2 phases. The increasing discrepancy between the LDA calculations and the experimental observations (MI, OI, and OII) may be due to the underestimation of the charge transfer from the O $2p$ states back to the Ti $3d$ states in LDA calculations. This observation is also supported with our and previous experimental work[1,9,10,33] that laser heating of TiO_2 at pressures above 25 GPa did not require a laser absorber and is likely related to the electronic Ti $3d$ states that become only accessible above this pressure for direct absorption of the infrared absorption. This interpretation is consistent with the observation that GGA (which includes the charge density gradient) predicts an EOS for the high-pressure OI and OII TiO_2 phases that is in good agreement with experiment [Figs. 4(e) and 4(f)]. We also note that Muscat et al.[34] used a triple-valence all-electron basis set which may localize $3d$ electrons more strongly on the Ti atoms in comparison to our plane-wave basis set. Thus, it appears that charge transfer from the O $2p$ to the Ti $3d$ states at least in TiO_2 phases at high pressures is likely enhanced.

In the stability field of OII, above $\sim$25 GPa we find good agreement between our experimental observations and our GGA calculations [Fig. 4(f)]. This is at variance with previous experimental observations of OII.[1] The volume decreases across the OI$\rightarrow$OII phase transition by $\sim$8.2% for LDA (transition pressure of 27 GPa) and by $\sim$7.6% for GGA (transition pressure of 38 GPa). However, the calculated volume changes using LDA or GGA depend only very weakly on pressure above 50 GPa, which is $\sim$7% in both approximations. This predicted large volume decrease is consistent with our experimentally determined large volume collapse of $\sim$8.3%. Furthermore, our predicted and observed large volume change is corroborated by the volume change across the OI$\rightarrow$OII transition in ZrO_2 and HfO_2 (Ref. 35) (Table V). In contrast, the EOSs in Refs. 1 and 10 suggest for the same transition a decrease in volume of $\sim$2.6%. Consequently, our EOS for OII is consistent with volume systematics across the OI$\rightarrow$OII transition and in very good agreement with our *first-principles* calculations. Additionally, at zero pressure, our GGA and LDA computations show that OII is denser than MI by $\sim$13% which compares well with our observations (9.9%) than what has been previously observed[1] (6.4%) on TiO_2 (Table IV).

V. CONCLUSIONS

We have investigated the structural phase transitions and the EOSs of TiO_2 under high pressure before and after heating at high temperature. Our EOSs compare well with previous observations for all TiO_2 phases except for OII where we observe a V_0 and K_0 that are significantly lower than obtained previously. Moreover, our experimental and theoretical results show that OII is a dense phase and that the volume across the OI$\rightarrow$OII is associated with a large volume collapse in good agreement to previous experiments and computations on similar dioxides.

ACKNOWLEDGMENTS

[1] L. S. Dubrovinsky, N. A. Dubrovinskaia, V. Swamy, J. Muscat, N. M. Harrison, R. Ahuja, B. Holm, and B. Johansson, Nature (London) **410**, 653 (2001).

[2] F. Iskandar, A. B. D. Nandiyanto, K. M. Yun, C. J. Hogan, K. Okuyama, and P. Biswas, Adv. Mater. (Weinheim, Ger.) **19**, 1408 (2007).

[3] J. Z. Hu, H. K. Mao, J. F. Shu, Q. Z. Guo, and H. Z. Liu, J. Phys.: Condens. Matter **18**, S1091 (2006).

[4] J. Z. Jiang, H. Lindelov, L. Gerward, K. Stahl, J. M. Recio, P. Mori-Sanchez, S. Carlson, M. Mezouar, E. Dooryhee, A. Fitch, and D. J. Frost, Phys. Rev. B **65**, 161202(R) (2002).

[5] A. Zerr, G. Miehe, G. Serghiou, M. Schwarz, E. Kroke, R. Riedel, H. FueB, P. Kroll, and R. Boehler, Nature (London) **400**, 340 (1999).

[6] T. Arlt, M. Bermejo, M. A. Blanco, L. Gerward, J. Z. Jiang, J. S. Olsen, and J. M. Recio, Phys. Rev. B **61**, 14414 (2000).

[7] L. Gerward and J. S. Olsen, J. Appl. Crystallogr. **30**, 259 (1997).

[8] W. Luo, S. F. Yang, Z. C. Wang, R. Ahuja, B. Johansson, J. Liu, and G. T. Zou, Solid State Commun. **133**, 49 (2005).

[9] M. Mattesini, J. S. de Almeida, L. Dubrovinsky, N. Dubrovinskaia, B. Johansson, and R. Ahuja, Phys. Rev. B **70**, 212101 (2004).

[10] N. A. Dubrovinskaia, L. S. Dubrovinsky, R. Ahuja, V. B. Prokopenko, V. Dmitriev, H.-P. Weber, J. M. Osorio-Guillen, and B. Johansson, Phys. Rev. Lett. **87**, 275501 (2001).

[11] V. Swamy, N. A. Dubrovinskaia, and L. S. Dubrovinsky, J. Alloys Compd. **340**, 46 (2002).

[12] J. M. Leger, J. Haines, A. Atouf, and P. Tomaszewski, in *High-Pressure Science and Technology*, edited by S. C. Schmidt, J. W. Shaner, G. A. Samara, and M. Ross (American Institute of Phys-

ics, New York, 1994), Vol. 309, p. 363.

[13] I. Fujishiro, G. J. Piermarini, S. Block, and R. G. Munro, in *Proceedings of the Eight AIRAPT Conference*, Uppsala, 1982, edited by C. M. Backman, T. Johannisson, and L. Tenger (ISBN, Sweden, 1982), Vol. II, p. 608.

[14] Y. Sato-Sorensen, J. Geophys. Res. **88**, 3543 (1983).

[15] D. L. Heinz and R. Jeanloz, Phys. Rev. B **30**, 6045 (1984).

[16] H. K. Mao and P. M. Bell, J. Appl. Phys. **49**, 3276 (1978).

[17] A. P. Jephcoat and S. P. Besedin, Philos. Trans. R. Soc. London, Ser. A **354**, 1333 (1996).

[18] A. P. Hammersley, S. O. Svensson, M. Hanfland, A. N. Fitch, and D. Hausermann, High Press. Res. **14**, 235 (1996).

[19] F. Birch, J. Geophys. Res. **57**, 227 (1952).

[20] R. Jeanloz, Geophys. Res. Lett. **8**, 1219 (1981).

[21] P. Hohenberg and W. Kohen, Phys. Rev. **136**, B864 (1964).

[22] G. Kresse and D. Joubert, Phys. Rev. B **59**, 1758 (1999).

[23] P. E. Blochl and M. Parrinello, Phys. Rev. B **45**, 9413 (1992).

[24] J. P. Perdew and A. Zunger, Phys. Rev. B **23**, 5048 (1981).

[25] J. P. Perdew, K. Burke, and M. Ernzerhof, Phys. Rev. Lett. **77**, 3865 (1996).

[26] G. Kresse and J. Furthmuller, Phys. Rev. B **54**, 11169 (1996).

[27] H. J. Monkhorst and J. D. Pack, Phys. Rev. B **13**, 5188 (1976).

[28] J. Haines, J. M. Leger, and O. Schulte, J. Phys.: Condens. Matter **8**, 1631 (1996).

[29] S. Desgreniers and K. Lagarec, Phys. Rev. B **59**, 8467 (1999).

[30] S. R. Shieh, A. Kubo, T. S. Duffy, V. B. Prakapenka, and G. Shen, Phys. Rev. B **73**, 014105 (2006).

[31] O. Ohtaka, H. Fukui, T. Kunisada, T. Fujisawa, K. Funakoshi, W. Utsumi, T. Irifune, K. Kuroda, and T. Kikegawa, Phys. Rev. B **63**, 174108 (2001).

[32] O. Ohtaka, H. Fukui, T. Kunisada, T. Fujisawa, K. Funakoshi, W. Utsumi, T. Irifune, K. Kuroda, and T. Kikegawa, J. Am. Ceram. Soc. **84**, 1369 (2001).

[33] R. Ahuja and L. S. Dubrovinsky, J. Phys.: Condens. Matter **14**, 10995 (2002).

[34] J. Muscat, V. Swamy, and N. M. Harrison, Phys. Rev. B **65**, 224112 (2002).

[35] J. E. Jaffe, R. A. Bachorz, and M. Gutowski, Phys. Rev. B **72**, 144107 (2005).

[36] D. L. Heinz and R. Jeanloz, J. Appl. Phys. **55**, 885 (1984).

[37] R. M. Hazen and L. W. Finger, J. Phys. Chem. Solids **42**, 143 (1981).

[38] J. K. Dewhurst and J. E. Lowther, Phys. Rev. B **54**, R3673 (1996).

[39] V. Swamy and B. C. Muddle, Phys. Rev. Lett. **98**, 035502 (2007).

[40] J. K. Dewhurst and J. E. Lowther, Phys. Rev. B **64**, 014104 (2001).

[41] M. A. Caravaca, J. C. Mino, V. J. Perez, R. A. Casali, and C. A. Ponce, J. Phys.: Condens. Matter **21**, 015501 (2009).